

SIMULATION OF THE F/A-18D "FALLING LEAF"

Paul T. Jaramillo* and John Ralston†
Bihrl Applied Research, Inc.
Hampton, Virginia 23666

Abstract

This paper discusses a phenomena which has been encountered on several of the today's strike and fighter aircraft. The motion can be described as violent, with angle-of-attack and sideslip angles traversing as much as 100 deg within a few seconds. The motion, unlike a spin, does not involve a continuous unidirectional heading angle change, but rather, displays an in-phase roll and yaw oscillation about a zero or small non-zero mean. This motion is produced by a complex interplay between dynamic and aerodynamic moments, and involves strong all-axis coupling. The details of this phenomena are discussed and six degrees-of-freedom simulations of the motion presented. The simulations have been evaluated against flight data.

Nomenclature

b	wingspan
c	mean aerodynamic chord
e_i	quaternion components
\mathbf{F}	vector of aerodynamic and propulsive force
F_i	aerodynamic and propulsive force component
g	gravity
I_{ii}	moments and products of inertia
L	rolling moment
M	pitching moment
m	mass
N	yawing moment
\tilde{q}	dynamic pressure
P	roll rate
Q	pitch rate
R	yaw rate
U	x axis velocity component
V	y-axis velocity component
\mathbf{V}	translational velocity vector
VAS	vertical airspeed
W	z-axis velocity component
α	angle-of-attack
β	sideslip
Ω	rotational velocity vector

*Research Engineer, Member AIAA

†Engineering Manager

This paper is declared a work of the U.S. Government and is not subject to copyright © Protection in the United States.

I. Introduction

The purpose of this paper is to describe the key features of a type of motion called the "falling leaf" and to delineate the basic requirements for its simulation. At present, there exist few works on this matter. The development of an operational definition of a new problem or phenomena is the first step to understanding it and solving it. In the case of the falling leaf, it appears that it may be just one of several closely related motions in a spectrum of out-of-control motions running from steady spins on one extreme to the falling leaf on the other. Furthermore, preliminary investigations show that the recovery techniques may vary considerably across this spectrum and therefore, such a problem definition is of practical importance.

II. System Modeling

Aircraft flight simulation involves the numerical calculation of the state of a dynamical system which is acted upon by external forcing functions, namely the aerodynamic, gravitational and propulsive forces and moments. As such, a typical flight simulation model has two major components: a set of relations which describe its dynamical and kinematical aspects, and a set of relations which describe its aerodynamical aspects. In addition, modern aircraft often contain complex control systems which, in effect, forms a third major component of the numerical model. In the following sub-sections, these three components will be briefly described.

2.1 Simulation Model

2.1.1 Aerodynamic Relations

The aerodynamic database used in this study is essentially a subset of the F-18C/D simulation data base version 3.0, currently in use at the Manned Flight Simulation (MFS) Center, Patuxent Naval Air Station. In this study, the high Mach functionality, for some of the aerodynamic components with more than three dimensions, was omitted because of the low speed flight regime examined as well as the need to reduce the database size for manipulation in the parametric study. The six aerodynamic components and their functionalities are depicted in Tables 1 and 2. The database itself is the evolution of an original

McDonnell Douglas F-18 simulation that has been the subject of much revision and validation since the first comparisons with flight were initiated at MFS in the 1980's.¹⁻⁷ The primary goals of these efforts have been to improve the database's low to mid speed range fidelity, through the use of flight and wind tunnel data, although many other flight regimes and store configurations were also examined. Structurally, the model was unified to make the original fragmented database continuous in angle-of-attack from -90° to +90°, and sideslip effects through 30° were added to most of the increments. Further, rotary damping terms, were also added to the simulation database. This data set was recently used in a study investigating

the significance of dynamic data mechanization schemes, wherein methods of combining wind axes and body axes damping terms in the simulation were evaluated against a wide range of flight test data for their ability to model dynamic motions.^{8, 9} The mechanization method recommended as a result of this study, a technique developed by Kalviste, was subsequently used in the simulation of the motions described in the following discussion.^{10, 11}

During the course of the work, some adjustments were made to more closely reproduce falling leaf motions. These changes primarily affected the high-angle-of-attack pitching moment characteristics but some static coefficients were estimated to 45 degrees of sideslip.

Table 1. Aerodynamic Force Increments

Increment	Functionality	Multplier	Remarks
DRAG			
CD basic	α, Mach		
CD fs	CL, Mach		full scale correction
DCD tf	Mach		trainer canopy
DCD clt	Mach		center-line tank
DCD int	Mach		interdiction loading
DCN int	α		$\text{DCD int} = \text{DCD int} + \text{DCN int} * \text{SIN}(\alpha)$
DCD lef	α, Mach	δ_{lef}	leading edge flap
DCD tef	α, Mach	δ_{tef}	trailing edge flap
DCD dhl, dhr	$\alpha, \delta_{hl} \text{ \& \ } \delta_{hr}$ separate		$\text{DCD dh} = (\text{DCD dhl} + \text{DCD dhr}) / 2$
DCN rot	$\alpha, \text{Sign}(\beta) * \Omega b / 2V, \beta $		$\text{DCD rot} * \text{SIN}(\alpha)$
DCN q	α, Mach	$Q_{osc} * c / 2V$	$\text{DCD q} = \text{DCN q} * \text{SIN}(\alpha)$
SIDE FORCE			
CY basic	α, β		
DCY tf	$\alpha, \beta $	$\text{Sign}(\beta)$	
DCY clt	$\alpha, \beta $	$\text{Sign}(\beta)$	
DCY int	$\alpha, \beta $	$\text{Sign}(\beta)$	
DCY lef	$\alpha, \beta $	$\text{Sign}(\beta) * \delta_{lef} / 25$	
DCY tef	$\alpha, \beta , \text{Mach}$	$\text{Sign}(\beta) * \delta_{tef} / 20$	
DCY dal, dar	$\alpha, \delta_{al} \text{ \& \ } \delta_{ar}$ separate		$\text{DCY ddf} = (\text{DCY dal} - \text{DCY dar}) * 2$
DCY dr	$\alpha, \delta_{rl} , \beta * \text{Sign}(\delta_r)$	$\text{Sign}(\delta_r)$	
DCY ddh	α, δ_h	δ_{dh}	$\delta_h = (\delta_{hl} + \delta_{hr}) / 2, \delta_{dh} = \delta_{hl} - \delta_{hr}$
DCY rot	$\alpha, \text{Sign}(\beta) * \Omega b / 2V, \beta $	$\text{Sign}(\beta)$	
DCY p	α, Mach	$\text{Posc} * b / 2V$	
DCY r	α, Mach	$\text{Rosc} * b / 2V$	
LIFT			
CL basic	α, Mach		
CL beta	$\alpha, \beta $		
DCN int	α		$\text{DCL int} = \text{DCN int} * \text{COS}(\alpha)$
DCL lef	α, Mach	δ_{lef}	
DCL tef	α, Mach	δ_{tef}	
DCL dal, dar	$\alpha, \delta_{al} \text{ \& \ } \delta_{ar}$ separate		$\text{DCL ddf} = \text{DCL dal} + \text{DCL dar}$
DCL dhl, dhr	$\alpha, \delta_{hl} \text{ \& \ } \delta_{hr}$ separate		$\text{DCL dh} = (\text{DCL dal} + \text{DCL dar}) / 2$
DCN rot	$\alpha, \text{Sign}(\beta) * \Omega b / 2V, \beta $		$\text{DCL rot} = \text{DCN rot} * \text{COS}(\alpha)$
DCL ad	α, Mach	$\alpha \text{ dot} * c / 2v$	alpha-dot
DCN q	α, Mach	$Q_{osc} * c / 2V$	$\text{DCL q} = \text{DCN q} * \text{COS}(\alpha)$

Table 2. Aerodynamic Moment Increments

Increment	Functionality	Multiplier	Remarks
ROLLING MOMENT			
Cl_basic	α, β		
DCl_off	α		static offset (non-zero at zero beta)
DCl_tf	$\alpha, \beta $	Sign(β)	
DCl_aim9	α	Kaim9 (= -1,0,1)	-1=Rt on, 1=Lt on, 0=both on/off
DCl_clt	$\alpha, \beta $	Sign(β)	
DCl_int	$\alpha, \beta $	Sign(β)	
DCl_ibpyl	α	β	
DCl_lef	$\alpha, \beta $	Sign(β)*(1- δ_{lef} / 34)	
DCl_tef	$\alpha, \beta , Mach$	Sign(β)*(1- δ_{tef} / 20)	
DCl_dal, dar	α, δ_{al} & δ_{ar} separate		DCl ddf = DCl dal - DCl dar
DCl_da_b	$\alpha, \beta, \delta_{df} $	Sign(δ_{df})	$\delta_{df} = (\delta_{al} - \delta_{ar}) / 2$
DCl_dr	$\alpha, \delta_r , \beta * \text{Sign}(\delta_r)$	Sign(δ_r)	
DCl_ddh	α, δ_h, β	δ_{dh}	$\delta_h = (\delta_{hl} + \delta_{hr})/2, \delta_{dh} = \delta_{hl} - \delta_{hr}$
DCl_rot	$\alpha, \text{Sign}(\beta) * \Omega b / 2V, \beta $	Sign(β)	
DCl_p	$\alpha, Mach$	Posc * b/2V	
DCl_r	$\alpha, Mach$	Rosc * b/2V	
PITCHING MOMENT			
Cm_basic	$\alpha, Mach$		
DCm_beta	$\alpha, \beta $		
DCm_clt	α		
DCm_int	α		
DCm_lef	$\alpha, Mach$	δ_{lef}	
DCm_tef	$\alpha, Mach$	δ_{tef}	
DCm_dal, dar	α, δ_{al} & δ_{ar} separate		DCm ddf = DCm dal + DCm dar
DCm_dr	$\alpha, \delta_r $	Sign(δ_r)	
DCm_dhl, dhr	α, δ_{hl} & δ_{hr} separate	δ_{dh}	DCm dh=(DCm_dhl + DCm_dhr)/2
DCm_rot	$\alpha, \text{Sign}(\beta) * \Omega b / 2V, \beta $		
DCm_ad	$\alpha, Mach$	$\alpha \cdot \dot{c} / 2v$	
DCm_q	$\alpha, Mach$	Qosc*c/2V	
YAWING MOMENT			
Cn_basic	α, β		
DCn_off	α		
DCn_tf	$\alpha, \beta $	Sign(β)	
DCn_aim9	α	Kaim9 (= -1,0,1)	-1=Rt on, 1=Lt on, 0=both on/off
DCn_clt	$\alpha, \beta $	Sign(β)	
DCn_int	$\alpha, \beta $	Sign(β)	
DCn_ibpyl	α	β	
DCn_lef	$\alpha, \beta $	Sign(β)*(1- δ_{lef} / 34)	
DCn_tef	$\alpha, \beta , Mach$	Sign(β)*(1- δ_{tef} / 20)	
DCn_dal, dar	α, δ_{al} or δ_{ar}		DCn ddf = DCn dal - DCn dar
DCn_da_b	$\alpha, \beta, \delta_{df} $	Sign(δ_{df})	$\delta_{df} = (\delta_{al} - \delta_{ar}) / 2$
DCn_dr	$\alpha, \delta_r , \beta * \text{Sign}(\delta_r)$	Sign(δ_r)	
DCn_ddh	α, δ_h, β	δ_{dh}	$\delta_h = (\delta_{hl} + \delta_{hr})/2, \delta_{dh} = \delta_{hl} - \delta_{hr}$
DCn_rot	$\alpha, \text{Sign}(\beta) * \Omega b / 2V, \beta $	Sign(β)	
DCn_p	$\alpha, Mach$	Posc * b/2V	
DCn_r	$\alpha, Mach$	Rosc * b/2V	

2.1.2 Automatic Flight Control System

The flight control system used in the following full-up simulation examples shown in this paper, was built to represent the up and away inner loop of the V8.3.3 F-18 control law mechanization.¹² Because of the flight regime examined, the outer loop functions, as well as the power approach logic and higher order structural filters, were not modeled in this study.

2.1.3 Dynamic and Kinematic Relations

The dynamic and kinematic relations used in the six degrees-of-freedom simulation are given in Eqs. (1) through (6). These are employed in a fourth-order numerical integration scheme in order to propagate the motion forward in time. The first set of equations, commonly referred to as the force equations, utilize quaternions to resolve the gravitational vector into the aircraft-carried axes. The forces, F_i , contain the aerodynamic and propulsive components. Mass was always assumed to remain constant on a given simulation run.

$$\begin{aligned}\dot{U} &= \frac{F_X}{m} + 2g(e_1 e_3 - e_0 e_2) + R V - Q W \\ \dot{V} &= \frac{F_Y}{m} + 2g(e_2 e_3 + e_0 e_1) + P W - R U \\ \dot{W} &= \frac{F_Z}{m} + g\{1 - 2(e_1^2 + e_2^2)\} + Q U - P V\end{aligned}\quad (1)$$

The moment equations are given in Eqs. (2) below. These equations do not account for any gyroscopic effects associated with the engines, mass shifting effects due to fuel sloshing or mass loss due to fuel consumption.

$$\begin{aligned}\dot{P} &= \left\{ \left(\frac{L}{I_{xx}} + \frac{I_{xz}N}{I_{zz}} \right) + \left(1 + \frac{I_{xx} - I_{yy}}{I_{zz}} \right) \frac{I_{xz}}{I_{xx}} P Q \right. \\ &\quad \left. + \left(\frac{I_{yy} - I_{zz}}{I_{xx}} - \frac{I_{xz}^2}{I_{xx}I_{zz}} \right) Q R \right\} \frac{I_{xx}I_{zz}}{I_{xx}I_{zz} - I_{xz}^2} \\ \dot{Q} &= \left\{ M + (I_{zz} - I_{xx}) P R + (R^2 - P^2) I_{xz} \right\} \frac{1}{I_{yy}} \\ \dot{R} &= \left\{ \left(\frac{N}{I_{zz}} + \frac{I_{xz}L}{I_{xx}} \right) + \left(\frac{I_{xx} - I_{yy}}{I_{zz}} + \frac{I_{xz}^2}{I_{xx}I_{zz}} \right) P Q \right. \\ &\quad \left. + \left(\frac{I_{yy} - I_{zz}}{I_{xx}} - 1 \right) \frac{I_{xz}}{I_{zz}} Q R \right\} \frac{I_{xx}I_{zz}}{I_{xx}I_{zz} - I_{xz}^2}\end{aligned}\quad (2)$$

The attitude equations shown in Eqs. (3) are necessary to update the quaternion components utilized in Eqs. (1) and (5). The use of quaternions is preferred over

other kinematical schemes for large-angle simulations because of their ability to perform all possible aircraft orientations in a singularity free manner. This is in contrast to the popular Euler angle schemes which have numerical difficulties when the aircraft's pitch angle reaches plus or minus 90 degrees as in a vertical climb or dive.

Quaternions, of course, have their own share of nuances, not the least of which is a general lack of usefulness of the quaternion components at the physical level. The simulation software provides relations which allow the Euler angles to be calculated from the quaternion components. The second nuance is of a mathematical nature. In particular, since the attitude equations employ four equations to calculate only three degrees-of-freedom, a constraint relationship is implied. Equation (4) provides this relationship. In particular, Eqs. (3) must be numerically propagated in such a manner so as to preserve the relationship between the quaternion components given by Eq. (4). Several techniques have been developed to accomplish this and in this work a constraint of the algebraic type was employed.¹³

$$\begin{Bmatrix} \dot{e}_0 \\ \dot{e}_1 \\ \dot{e}_2 \\ \dot{e}_3 \end{Bmatrix} = \frac{1}{2} \begin{bmatrix} e_0 & -e_1 & -e_2 & -e_3 \\ e_1 & e_0 & -e_3 & e_2 \\ e_2 & e_3 & e_0 & -e_1 \\ e_3 & -e_2 & e_1 & e_0 \end{bmatrix} \begin{Bmatrix} 0 \\ P \\ Q \\ R \end{Bmatrix}\quad (3)$$

$$e_0^2 + e_1^2 + e_2^2 + e_3^2 = 1\quad (4)$$

Finally, the navigation equations given in Eq. (5) allow the calculation of the trajectory of the aircraft through the atmosphere. For the present work, only the last equation was utilized since the numerical model is not affected by the aircraft's spatial position with the exception of its altitude. The third component is therefore modified as in Eq. (6) in order to provide the necessary information for the standard atmosphere model.

$$\begin{Bmatrix} \dot{X} \\ \dot{Y} \\ \dot{Z} \end{Bmatrix} = \begin{bmatrix} 1-2(e_2^2+e_3^2) & 2(e_1e_2-e_0e_3) & 2(e_1e_3+e_0e_2) \\ 2(e_1e_2+e_0e_3) & 1-2(e_1^2+e_3^2) & 2(e_2e_3-e_0e_1) \\ 2(e_1e_3-e_0e_2) & 2(e_2e_3+e_0e_1) & 1-2(e_1^2+e_2^2) \end{bmatrix} \begin{Bmatrix} U \\ V \\ W \end{Bmatrix}\quad (5)$$

$$\dot{H} = -\dot{Z}\quad (6)$$

III. OVERVIEW OF THE FALLING LEAF

3.1 General Characteristics of Falling Leaf Motions

Table 3 illustrates some general kinematical characteristics of the falling leaf in relation to other out-

of-control motions. The first row of comments in the table compares the most prominent rotational velocity components of the falling leaf in relation to steady and oscillatory spins. The second row compares the translational velocity vector through the aerodynamic angles. The fact that many of the falling leaf motions tend to look like oscillatory spins has led some to naming these motions as low- or intermediate- mode oscillatory spins. Although this view is certainly acceptable, distinctions between these motions are important, because, unlike oscillatory spins experienced by this aircraft, the motions discussed in this paper do not share the characteristic of being relatively easy to recover from. In fact, due to the yaw rate behavior during the falling leaf, spin arrows displayed while in spin recovery mode have given pilots intermittent and confusing information during such motions. The recognition that a “spectrum” of out-of-control motions exist, which at once recognizes the similarities and the differences between these motions, may serve to make control system designers aware of the broader spectrum of out-of-control motions which must be dealt with.

Table 4 summarizes the main characteristics of falling leaf motions in terms of some key variables. In general, the motions can be divided into two general categories: slow falling leaf motions and fast falling leaf motions. The primary differences in going from the slow to the fast motions (darker highlight) can be seen in the movement of the angle-of-attack trace to higher values, the biasing of the yaw rate and a decrease in the period of the motion, i.e. increase in the frequency of oscillation. Simulations indicate that fast falling leaf motions do not divide along such distinct borders but rather occur in a spectrum which primarily involves further increases in the minimum angle-of-attack of the motion while maintaining the same angle-of-attack range, i.e. approximately 60 degrees between the minimum and maximum angles. Secondary differences include small increases in the magnitudes of the yaw and pitch rates. These differences are indicated by the lighter highlight.

Table 3. Spectrum of Post-Stall Gyration

FALLING LEAF	OSCILLATORY SPIN	STEADY SPIN
In-Phase, Periodic Roll and Yaw Rates Fluctuating about Small or Zero Means.	In-Phase, Periodic Roll and Yaw Rates Fluctuating about Large Non-Zero Means.	Steady Roll and Yaw Rates At Large Non-Zero Values.
Large α and β Fluctuations Yielding Large peak $\dot{\alpha}$ and $\dot{\beta}$. Angle-of-Attack May Dip Below Stall Angle.	Moderate α Fluctuations but β Fluctuations may be Large: Moderate $\dot{\alpha}$ and $\dot{\beta}$ Aircraft remains Stalled throughout Motion	Small α or β Fluctuations Yielding Minimal $\dot{\alpha}$ and $\dot{\beta}$. Aircraft Remains in a Deep Stall

Table 4. Falling Leaf as a Sub-Spectrum of Post-Stall Gyration

STATE	SLOW FALLING LEAF	FAST FALLING LEAF	HIGH ALPHA FAST FALLING LEAF
α (deg)	-5 to +60	+20 to +70	+30 to +85
β (deg)	-40 to +40	-40 to 40	-40 to +40
P (deg/sec)	-120 to +150	-90 to +130	-90 to +130
Q (deg/sec)	-30 to +30	-35 to +35	-50 to +50
R (deg/sec)	-50 to +50	-10 to +60	-10 to +75
λ (sec)	7	4.7	4.5
$\dot{\alpha}$ (deg/sec)	70	70	70
$\dot{\beta}$ (deg/sec)	100	100	100
H dot (fps)	350	325	325

Whereas the shift in the angle-of-attack range may impact the effectiveness of the controls, the higher rotational rates about the pitch and yaw axes result in higher momentum and energy levels. This can impact the ease of- or time required for- recovery due to a difference in the level of energy which must be dissipated to attenuate the motion. The existence of a

sub-spectrum of falling leaf motions within the larger spectrum of post-stall gyration, raises questions as to whether or not one recovery system can work for all motions. It is even possible that a recovery system or technique capable of stopping one type of motion, may actually aggravate other motions in the spectrum.

Figure 1 provides and a rare, high-quality flight-test record of a slow falling leaf motion. The first four graphs provide the aerodynamic angles, rotational velocity components, Euler angles and speed in that order. The next four graphs show the rudder, left and right aileron, left and right horizontal stabilizers, and altitude, again in that order. Although the motion depicted in this figure cannot be considered as having reached a “steady state” condition, there are several characteristics which are evident and become more clearly defined during sustained motions.

First, note that the aircraft spends most of the time in a very high sideslip condition or in a high angle-of-attack coupled with a high sideslip condition. Simulation databases of many military aircraft may cover a large angle-of-attack range but tend to lack high sideslip data. Without high sideslip data coverage, at least in the basic static coefficients, there is little chance of simulating the motion. In addition, most of the controls show strong dependence on both of the aerodynamic angles so that the database must also include high sideslip controls data. The controls data requirements are necessary, not only for properly simulating the motion, i.e. automatic flight control systems may play a large role in the motion, but also to allow a credible analysis of recovery options. The other distinguishing feature can be seen in the overplots of the roll and yaw rates. In particular, these two states display an in-phase behavior throughout the motion.

Figure 2 provides a time history of a simulated motion referred to in this paper as a “fast falling leaf.” The motion begins as a slow falling leaf similar to that shown in Figure 1 until the controls are held neutral at 30 seconds. The oscillations are seen to speed up for about two cycles then slow down again for another half a cycle. At around 40 seconds, the motion finally begins to sustain itself in a higher frequency oscillatory mode. The period of motion decreases from just under 8 seconds in the slow pattern to just under 5 seconds in the fast motion. The relationships between the state variables settle down into distinct patterns, although in true non-linear fashion, the states never exactly repeat themselves. Notice that the angle-of-attack range of the motion shows some variation with time even in the “steady state” portion of the motion.

A strong biasing of the yaw rate also distinguishes this type of motion from the slow motion depicted in Figure 1. Although the yaw rate actually reverses itself during the motion, the bias results in a near continual heading change resembling an oscillatory spin. This is clearly seen in the trace of Psi, the Euler heading angle shown in the third graph Figure 2. This behavior led some to naming this motion a low- or intermediate- mode oscillatory spin. In the sustained motion, a pattern does

become visible in the pitch rate trace, and it can clearly be seen as lagging behind the roll and yaw traces. This is due to the influence of the inertial pitch acceleration component, which is highest when the roll and yaw rates are at their peak. Since the rate is the integral of the acceleration, this lag is expected; and is also an indication of the strength of the inertial pitch acceleration term.

Figure 3 depicts a simulation of a motion which is being termed a “high-alpha fast falling leaf” in this paper. Like the motion depicted in Figure 2, the angle-of-attack range is not precisely fixed, but in this case slowly drifts upward even once the motion has reached a repeatable pattern beyond about 35 seconds. The relationships between the states are not appreciably different from the fast falling leaf shown in Figure 2. Subtle changes are noted, however, such as a slight change in the pitch rate behavior as well as a small increase in the pitch and yaw rates. The consequences of this seemingly small shift can be seen in the trace of the magnitude of the angular momentum vector which is shown in the last graph of Figures 2 and 3. A correlation can be made between the angle-of-attack range of the motion and the area below the angular momentum curve. In particular, as the angle-of-attack drifts towards higher values, the average angular momentum increases. Since this momentum must be overcome to stop the motion, this feature should be expected to affect recovery.

3.2 Simulation vs. Flight

This section addresses the accuracy to which the falling leaf motion could be simulated using the model and methodology described in section 2. In doing so, it also establishes the extent to which conclusions based on such work can be considered as reliable. Unfortunately, there existed very few flight-test data of sufficient quality against which the accuracy of the simulation could be measured. Figure 4 compares a few features of Flight 12-9, seen previously in Figure 1, and a simulation run driven only by the recorded pilot stick and rudder inputs. Considering the nature of the motion, the agreement is excellent in terms of the magnitudes and phasings between the states; and the fact that the simulation showed a similar recovery.

Figure 5, provides an example of the ability of the model to produce fast falling leaf motions. Unfortunately, a set of high-quality data for this type of motion was not available for this study. However, reference 14 provided a hand-rendered time history of a motion experienced by an F-18A, which, at the time was called an “intermediate yaw rate oscillatory spin.”

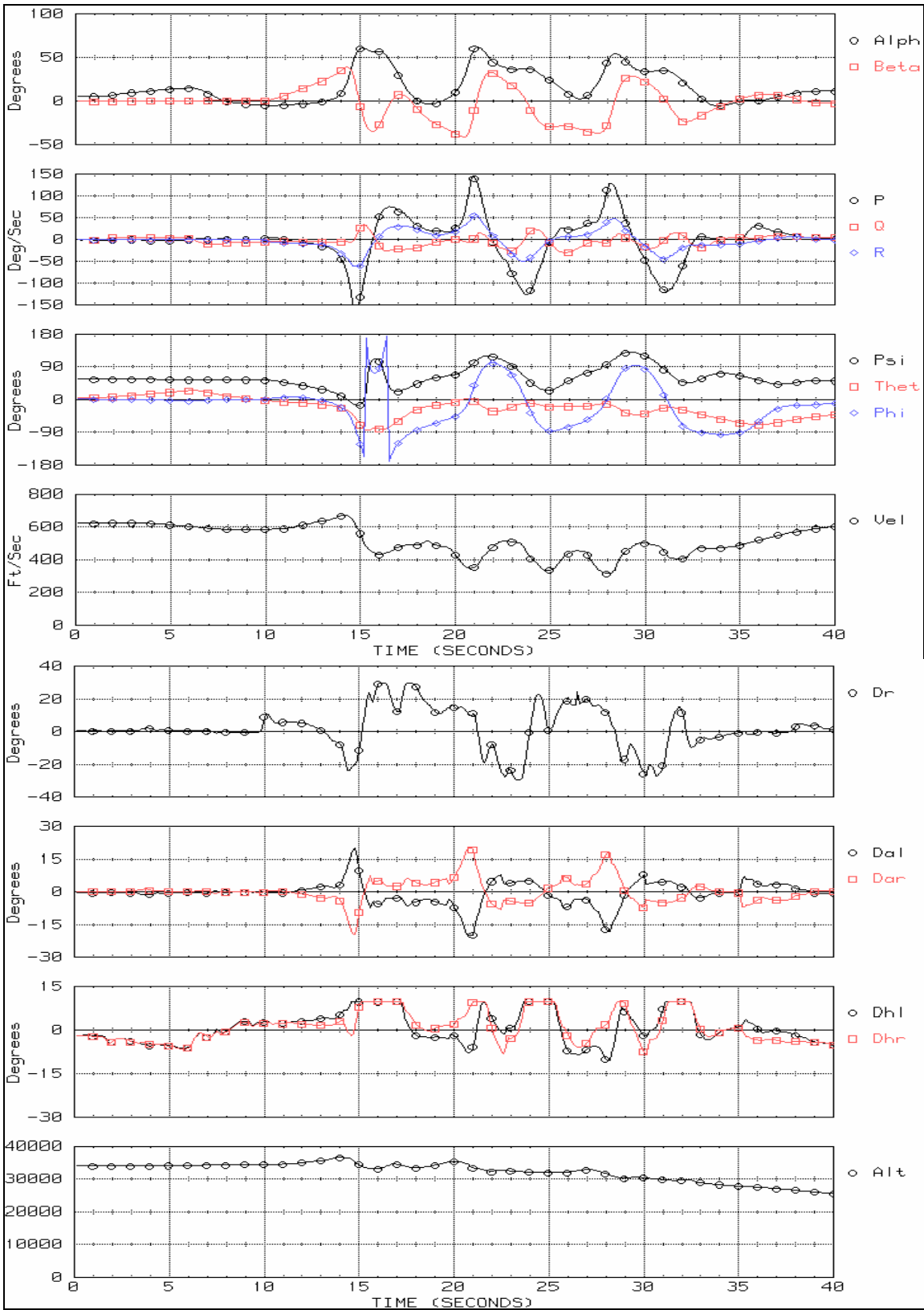


Figure 1. Flight 12-9: Slow Falling Leaf

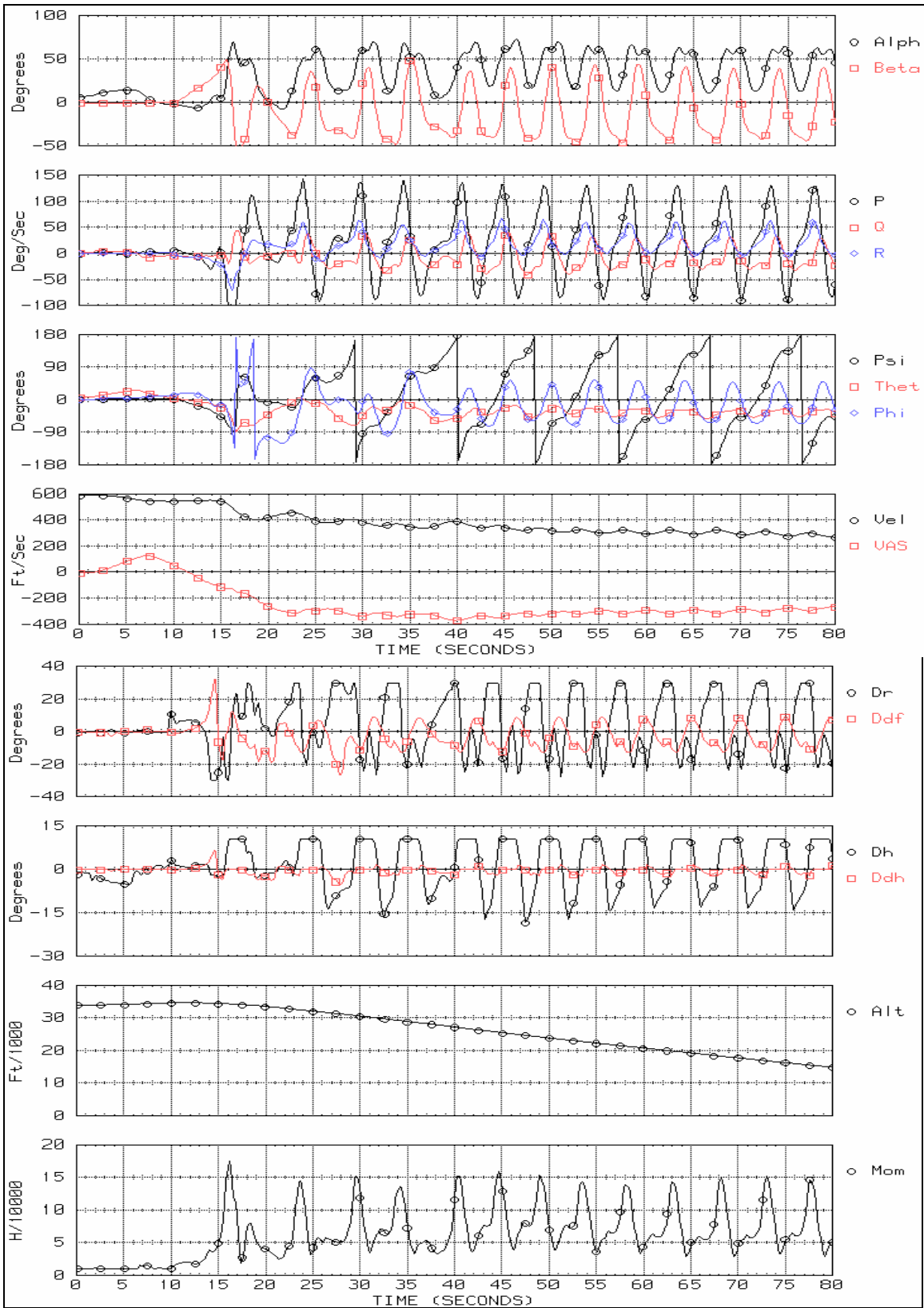


Figure 2. Simulation of a Fast Falling Leaf

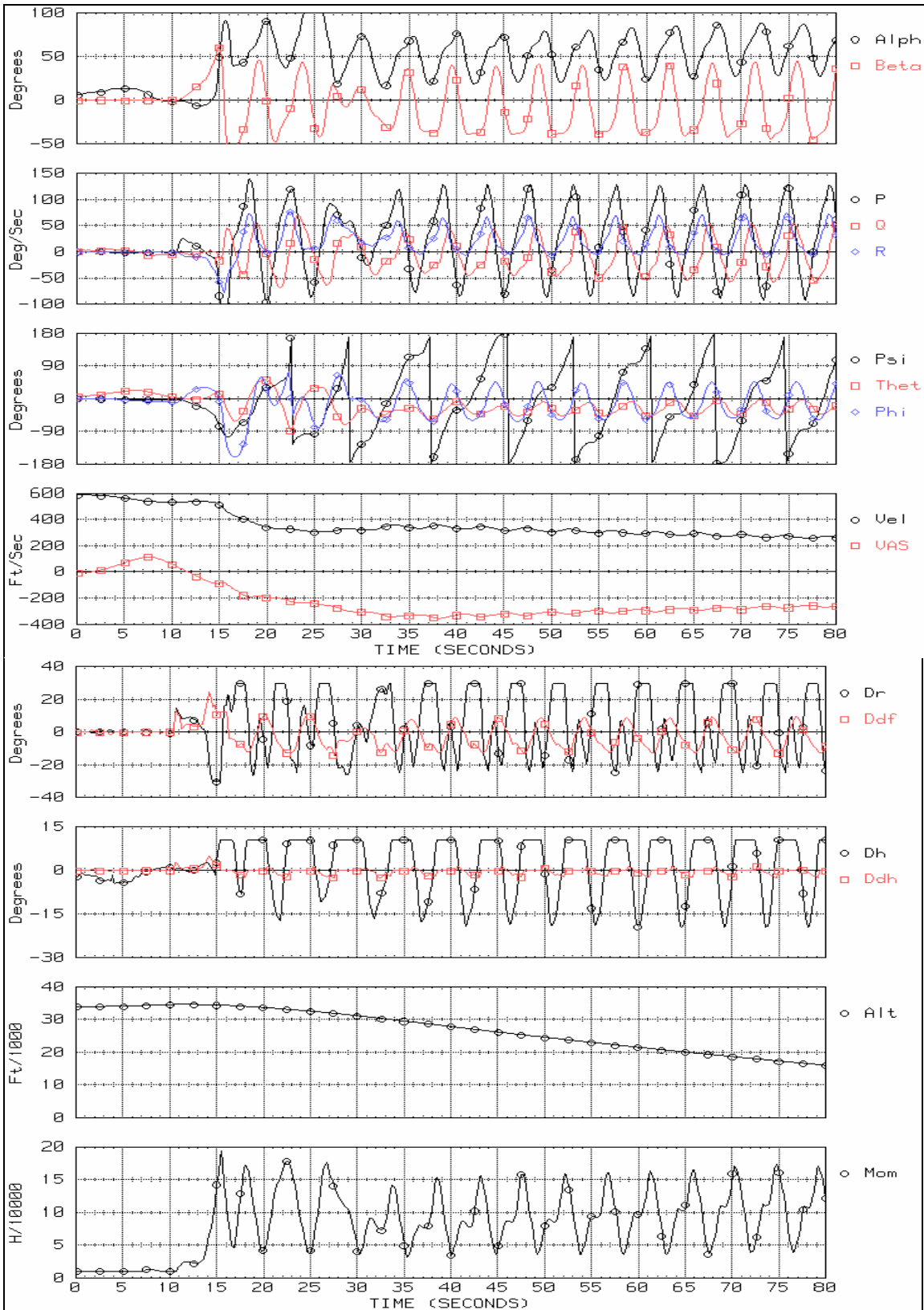


Figure 3. Simulation of a High-Alpha Fast Falling Leaf

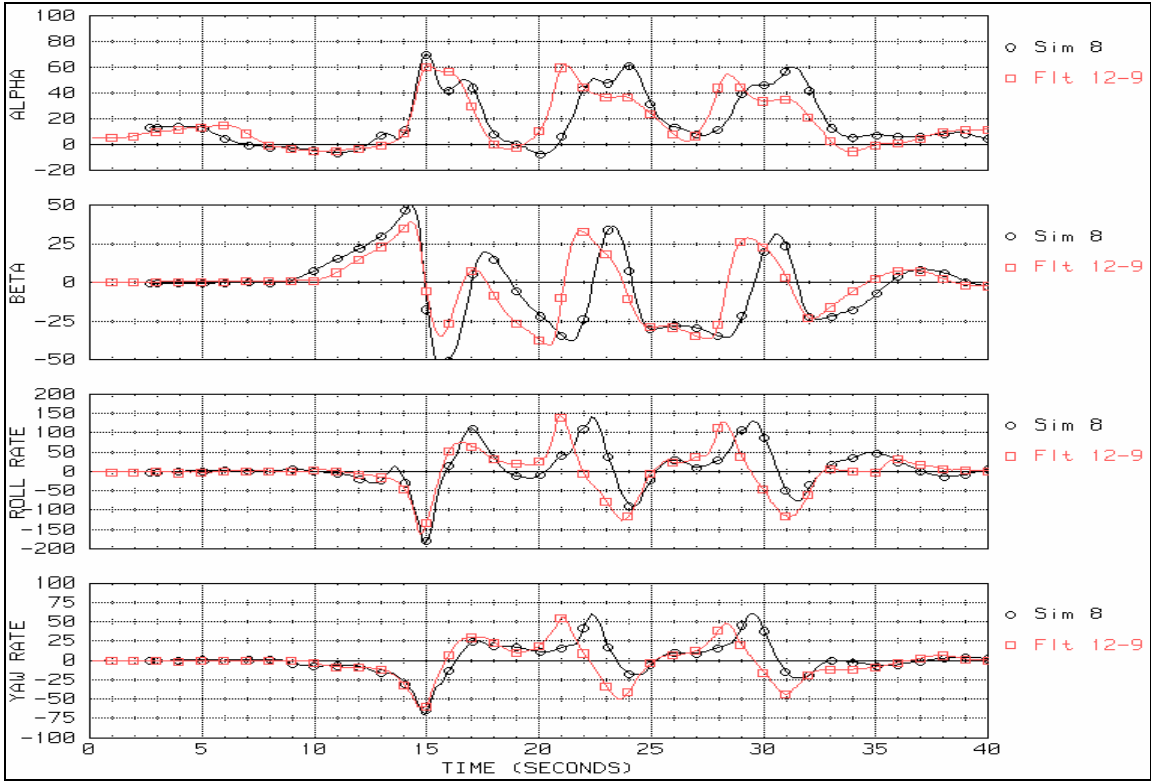


Figure 4. Flight 12-9 vs. Simulation

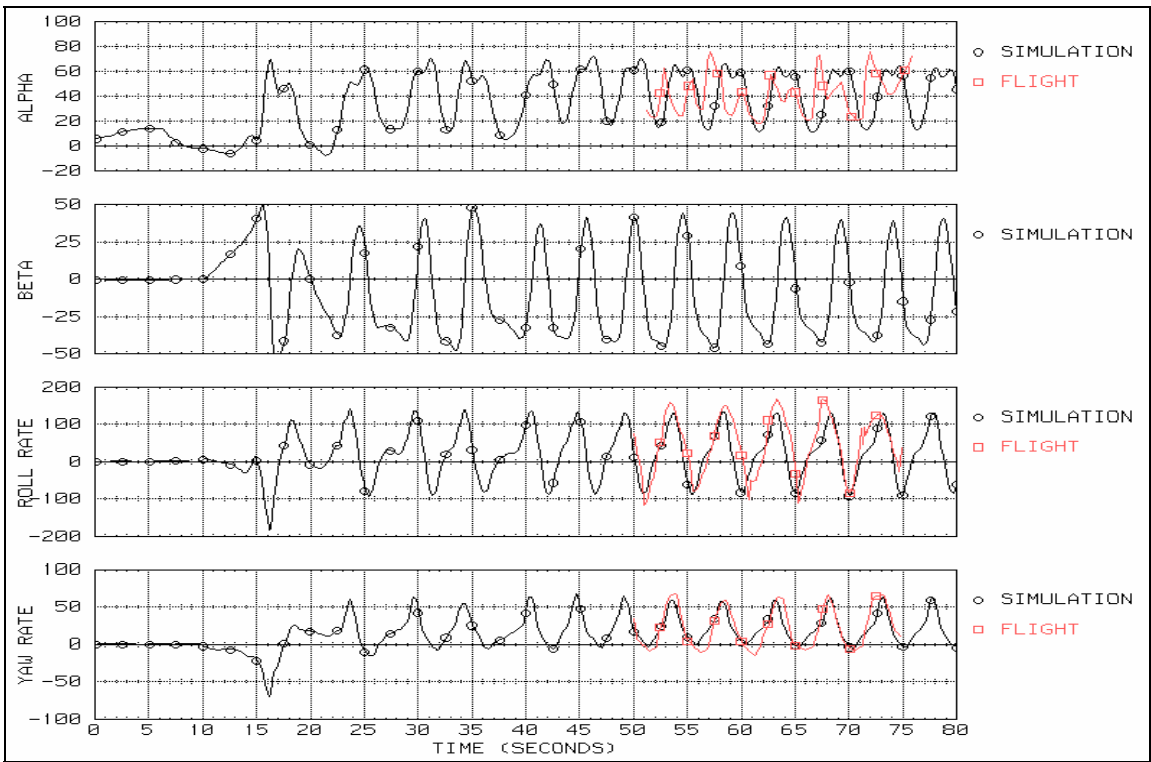


Figure 5. F-18A Flight Record vs. Simulation

To prepare Figure 5, the data traces of the flight record were retraced and scanned into the computer. The

angular rates were inverted to change the flight record from a left motion to a right motion. The middle 25 seconds of the motion were selected to emphasize the most salient points. Any attempt to simulate the entire flight would have been very difficult given the quality of the data, the sensitivity of the motion to the initial conditions, and the lack of key configurational data. The correlation of the simulation with the available states recorded during this flight, and general comparisons with falling leaf traces from other aircraft, indicate that the simulation provides a reasonably accurate portrayal of this type of motion.

In evaluating the accuracy of the simulation, it must be kept in mind that practically the entire simulation database is excited by these motions. In particular, the angle-of-attack ranges between slightly negative angles to over 70 degrees while the sideslip angle ranges between plus and minus 40 degrees. The wide range of angular rates also excites a large portion of the rotational and dynamic database. In sum, the accuracy of the simulation model is sufficient to allow a detailed analysis of the motion; and results should be considered to have a high degree of reliability.

IV. Concluding Remarks

This work has illustrated that very complex motions such as the falling leaf can be modeled with sufficient accuracy given a comprehensive aerodynamic database and an accurate automatic flight control system model. The minimal database requirements include high sideslip data in the static coefficients: at least up to 45 degrees, and preferably up to 60 degrees. Accurate simulation also requires a strong complement of rotary balance and forced oscillation data. In order to provide a credible analysis of recovery, data on controls effectiveness at high sideslip is also essential.

Acknowledgments

The authors wish to express their gratitude to Bill McNamara and Chad Miller at NAWC/AD Manned Flight Simulation Facility for their support of this work.

References

1. Hess, R. A., "Simulation Checking Using an Optimal Prediction Evaluation (SCOPE) User Guide," SCT Rept. 4522-270-2, September 1987.
2. Hess, R. A., "Subsonic F/A-18A and F/A18A/B Aerodynamic Identified from Flight-Test Data," Rept No. SCT-4522-220-1, July 1987.
3. Ralston, John N., "Analysis of F-18A/B Low Speed, High Angle-of-Attack Aerodynamic Data Base, Bar 88-7, September 1988.
4. Hess, R. A., "Effect of Various Stores on the Aerodynamics of an F/A-18B Aircraft Aerodynamic Identified from Flight-Test Data," Rept No. SCT-6612-020-2, February 1989.
5. O'Conner, Cornelius, "NATC F-18A/B Aerodynamic Math Model Modifications Incorporated during the Phase I Model Unification Effort," BAR 89-5, March, 1989.
6. O'Conner, Cornelius, "NATC F-18A/B Aerodynamic Math Model Modifications Incorporated during the Phase II Model Unification Effort," BAR 90-13, September, 1990.
7. Ralston, John N. and Avent, J. L., "Evaluation and Modification of F/A-18B Aerodynamic Data Base for Improved Departure Modeling, BAR 92-2, Mar. 1992.
8. Ralston, John N., O'Connor, C. J. and Avent, J. L., "Evaluation of the NAWC/AD F/A-18 C/D Simulation Including Data Base Coverage and Dynamic Data Implementation Techniques," BAR 95-3, Dec. 1995.
9. O'Connor, C. J., Ralston, John N., and Timothy Fitzgerald, "Evaluation of the NAWC/AD F/A-18 C/D Simulation Including Data Base Coverage and Dynamic Data Implementation Techniques," AIAA Paper 96-3365, May 1996.
10. Kalviste, Juri, "Use of Rotary Balance and Forced Oscillation Test Data in a Six Degrees-of-Freedom Simulation," AIAA Paper 82-1364, Aug. 1982.
11. Kalviste, Juri, "Math Modeling of Aero Data for Aircraft Dynamic Motion" AIAA 94-AFM-26-7, August 1994.
12. Glaser, B., Hess R. K., Trame, L. W., "F/A-18 V8.33 Control Law Mechanization," McDonnell Douglas Memo 338-5788, May 1984.
13. Bach, Ralph, Russell Paielle, "Direct Inversion of Rigid Body Rotational Dynamics," NASA TM-102798, 1990.
14. McNamara, William, "F/A-18A Intermediate Yaw Rate Oscillatory Spin Requiring Manual SRM Recovery," Memorandum, October 9, 1987.